

To be appeared in The Astrophysical Journal April 20, 1999 issue
(Vol. 515)

The Radio Emission of the Seyfert Galaxy NGC 7319 ¹

Kentaro Aoki

Astronomical Data Analysis Center, National Astronomical Observatory of Japan,
2-21-1, Osawa, Mitaka, Tokyo 181-8588 Japan

George Kosugi

Subaru Telescope, National Astronomical Observatory of Japan,
650 North A'ohoku Place, Hilo, HI 96720

Andrew S. Wilson²

Astronomy Department, University of Maryland, College Park, MD 20742-2421

and

Michitoshi Yoshida

Okayama Astrophysical Observatory, National Astronomical Observatory of Japan,
Kamogata-cho, Asakuchi-gun, Okayama 719-0232, Japan

ABSTRACT

We present VLA maps of the Seyfert 2 galaxy NGC 7319 at 3.6, 6, and 20 cm. Sub-arcsecond resolution is achieved at 3.6 and 6 cm. The radio emission exhibits a triple structure on a scale of $\sim 4''$ (1.7 kpc). All three components have steep spectra, consistent with synchrotron radiation. We have also analyzed an *HST* archival, broad-band red image, which contains structure related to the radio components. In particular, a V-shaped feature in the HST image some $3''.7$ (1.6 kpc) southwest of the nucleus is associated with highly blueshifted emission lines seen in ground-based spectra. We interpret the V-shaped feature as emission from gas compressed by the bow shock driven by the outwardly moving radio plasmoid.

Subject headings: galaxies: active — galaxies: individual (NGC 7319) — galaxies: nuclei — galaxies: Seyfert — radio continuum: galaxies

¹Based on observations made with the Very Large Array operated by the National Radio Astronomy Observatory and on observations made with the NASA/ESA Hubble Space Telescope, obtained from the data archive at the Space Telescope Science Institute, which is operated by the Association of Universities for Research in Astronomy, Inc., under NASA contract NAS 5-26555.

²Adjunct Astronomer, Space Telescope Science Institute

1. INTRODUCTION

A number of investigations have been made of the relationship between the radio emission and the narrow-line regions (NLR) of Seyfert galaxies. From ground-based observations, it is found that the NLR are aligned and cospatial with the radio emission (Haniff, Wilson, & Ward 1988). There is also evidence that the kinematics of the NLR are related to the radio-emitting plasma. Whittle et al. (1988) studied [O III] $\lambda 5007$ emission-line profiles in several Seyfert galaxies which have linear (i.e. double, triple or jet-like) radio sources. They found that substructures (subpeaks and shoulders) in the line profiles are more conspicuous close to the radio components. This result suggests that the radio-emitting plasma interacts with the optical line-emitting gas.

The *Hubble Space Telescope* (*HST*) has allowed much higher resolution imaging of the NLR and several studies have focussed on the relationship between the NLR and the radio emission (Bower et al. 1994, 1995; Capetti et al. 1996; Capetti, Macchetto & Lattanzi 1997; Falcke, Wilson & Simpson 1998). These observations have shown detailed correspondences between optical emission-line and radio continuum images, and indicate that interactions between radio plasma and the ambient gas determine the morphology of the NLR, with the radio ejecta sweeping up and compressing the interstellar medium. Detailed observations of such interactions are, therefore, necessary to understand the NLR within several hundreds pc of the nucleus.

NGC 7319, a member of Stephan’s Quintet, is a type 2 Seyfert galaxy with circumnuclear, outflowing, ionized gas which aligns with the radio emission (Aoki et al. 1996). Multiple components are found in the optical emission-line profiles on the SW side of the nucleus. The velocity of the outflow ranges up to 500 km s^{-1} and its extent is 4 kpc. NGC 7319 thus exhibits one of the largest circumnuclear outflows known in Seyfert galaxies.

In this paper, we report sub-arcsecond resolution radio imaging of NGC 7319 with the Very Large Array (VLA). These radio images are compared to an *HST* archival broad-band WFPC2 image and the results of ground-based optical spectroscopy by Aoki et al. (1996) in order to study in detail the relationship between the radio emission and the outflowing gas. Our VLA observations and the HST image are described in Section 2. The results are presented in Section 3, while in Section 4 we discuss the properties of the radio-emitting plasma in NGC 7319 and interpret our results. We give concluding remarks in Section 5. The heliocentric systemic velocity of 6740 km s^{-1} (Aoki et al. 1996) gives a distance of 86 Mpc for NGC 7319 assuming a Hubble constant $H_0=75 \text{ km s}^{-1} \text{ Mpc}^{-1}$ and the solar motion relative to the CMB radiation field (Smoot et al. 1991). Thus $1''$ corresponds to 420 pc.

2. OBSERVATIONS AND REDUCTION

2.1. VLA Data

The VLA observations of NGC 7319 were made in the ‘A-configuration’ at 20, 6 and 3.6 cm on 1996 November 4. The integration times on NGC 7319 were 1.4, 1.3, and 1.2 hours at 20, 6, and 3.6 cm, respectively. Each 6 and 3.6 cm band consisted of two contiguous channels with a total bandwidth of 100 MHz centered at 4860 and 8440 MHz, respectively. Two separate 50 MHz channels centered at 1365 and 1435 MHz were used for the 20 cm observations. The data were phase calibrated by means of observations of the source 2236+284, which is 6′ away from NGC 7319. The calibrator and NGC 7319 were observed sequentially with a 15 min cycle. Flux calibration was achieved by observations of 3C48.

Data reduction was done with AIPS in Socorro. The observations of NGC 7319 were flux and phase calibrated, mapped, and CLEANed to give the final images. Due to an error, we observed 3C48 at 1385 and 1465 MHz, which are different from the 20 cm bands used for NGC 7319 and 2236+284. The fluxes of 2236+284 at its observed frequencies of 1365 and 1435 MHz were therefore determined by interpolation and extrapolation of the 3C 48 observations, and used to flux calibrate the observations of NGC 7319.

2.2. HST Data

There is a broad-band image of NGC 7319 in the *HST* archive. It was obtained with WFPC2 through the filter F606W (effective wavelength/width 5843 Å/1578.7 Å). The nuclear region of NGC 7319 was imaged with the Planetary Camera, which has a pixel size of 0′′.0455. Bias and dark subtraction, and flat fielding were done with pipeline processing at the Space Telescope Science Institute. We removed cosmic ray events from the data using IRAF³. Note that the F606W filter contains strong emission-lines, such as [O III] λ 5007, H α , and [N II] λ 6584, from NGC 7319. The system throughputs at [O III] λ 5007 and H α are 60 % and 90 % of the peak, respectively, so the structures in this image are influenced by emission-lines.

3. RESULTS

3.1. Radio Images

The full resolution 3.6, 6, and 20 cm maps are presented in Figure 1, 2, and 3, respectively. Three compact components, plus diffuse emission, are visible in the higher resolution maps. The positions, flux densities, and sizes (FWHM) of the compact components were measured using

³IRAF is distributed by the National Optical Astronomy Observatories, which are operated by the Association of Universities for Research in Astronomy, Inc. under cooperative agreement with the National Science Foundation.

the AIPS task JMFIT, which is a two-dimensional elliptical gaussian fitting program. These parameters are summarized in Table 1. The sizes are given after deconvolution from the beams.

In the highest resolution ($0''.27 \times 0''.26$ FWHM) map (Fig. 1), the three compact components, labeled A, B and C, are found to be aligned in P.A. $24 \pm 1.4^\circ$. The separations of A and B, B and C, A and C are $0''.97$ (410 pc), $3''.36$ (1.4 kpc), and $4''.32$ (1.8 kpc), respectively. Component A has a size of $0''.3 \times 0''.2$ (130 pc \times 80 pc) and is elongated in P.A. $\sim 0^\circ$. Component C has a size of $0''.25 \times 0''.2$ (110 pc \times 80 pc) and is elongated in P.A. $\sim 40^\circ$. There is a diffuse component which extends $\sim 2''$ towards the north from C. There is also diffuse emission extending to the south of A.

The structure in the 6 cm naturally weighted map ($0''.47 \times 0''.45$ FWHM) (Fig. 2) is similar to that in the 3.6 cm map. The three components (A, B, and C) are clearly seen, with diffuse emission extending between A and C. The overall appearance of two outer ‘hot spots’ (A and C) with diffuse emission extending back towards the nucleus is reminiscent of FR II-class radio galaxies, though with much lower radio power and smaller spatial extent in NGC 7319.

The A and B components which are seen in the 3.6 cm and 6 cm images are merged together in the 20 cm uniformly weighted image ($1''.31 \times 1''.29$ FWHM) (Fig. 3). The position of this merged peak agrees with that given by van der Hulst & Rots (1981) to within $0''.2$. The resolution of our 20 cm image is higher than that of van der Hulst & Rots (1981), and the jet-like feature seen in their Figure 3 corresponds to our component C. Our 20 cm total flux density of 28.5 ± 0.5 mJy agrees with that found by van der Hulst & Rots (1981).

The spectral indices (α : $f_\nu \propto \nu^\alpha$) of the three compact components were calculated from the 3.6 and 6 cm flux densities and are given in Table 1. The spectral index between 20 and 6 cm is also derived for component C. The spectral indices of all three components are similar ($\alpha \sim -1.3$). Our derived spectra for components with diffuse emission may be systematically too steep as the shorter wavelength maps may miss extended flux. However, the steep spectra are consistent with the spectral index of the total radio emission ($\alpha = -1.2$, van der Hulst & Rots (1981); $\alpha = -1.1 \pm 0.3$, Kaftan-Kassim, M. A., Sulentic, J. W., & Sistol, G. (1975)).

3.2. Optical Image

The *HST* F606W image of NGC 7319 is shown in Figure 4. Prominent spiral-like structure is seen around the nucleus. The spiral features extend $1''.4$ (590 pc) to the north and $1''$ (420 pc) to the south of the nucleus. The northern arm is associated with a dust lane. There is also a V-shaped feature $3''.4$ south and $1''.4$ west of the nucleus. To enhance the contrast of the fine-scale structure, we smoothed the image with a gaussian function of $1''.5$ FWHM and subtracted it from the original (unsmoothed) one. The difference image is shown in Figure 5. The V-shaped feature, as well as the spiral-like structure mentioned above, are clearly seen.

Both the spiral-like structure and the V-shaped feature may, at least in part, be emission-line

regions, since strong emission-lines ([O III] λ 5007, $H\alpha$, and [N II] λ 6584) are present in the filter passband. We have estimated the contribution of emission-lines to the spiral-like structure and the V-shaped feature in the F606W image using ground-based spectra of the corresponding region. Nuclear (aperture size $4''.4$ in NS \times $1''.8$ in EW) and off-nuclear (aperture size $1''.8$ in NS \times $4''.4$ in EW) spectra were extracted. The two extraction windows include the spiral-like structure and the V-shaped feature, respectively. These spectra were multiplied by the transmissions of *HST*, WFPC2 and F606W using the synthetic photometry package SYNPHOT in STSDAS. The result is that emission lines contribute 17 % and 3 % of the total flux of the nuclear region and off-nuclear region, respectively. We also derived the fluxes in the *HST* original (Fig. 4) and difference (Fig. 5) images within the same apertures as used to extract the ground-based spectra. The spiral-like structure (as measured from the difference image) comprises 14% of the total flux (from the original image) through the nuclear aperture. The corresponding number for the V-shaped feature through the off-nuclear aperture is 3%. These fractions are similar to the contributions of emission-lines in each aperture, so it is possible that both structures are emission-line features with the smoothly distributed background being stellar light.

4. DISCUSSION

4.1. The Physical Properties of Radio Plasma

Double or triple radio structures similar to NGC 7319 are found in many Seyfert galaxies (Ulvestad & Wilson 1984a, 1984b, 1989; Kukula et al. 1995). The steep spectra of the three compact components in NGC 7319 are consistent with synchrotron radiation. Adopting the minimum energy condition for cosmic rays plus magnetic field, we have estimated the magnetic field strength for components A and C. We have assumed power-law spectra ($\alpha = -1.2$ for A, $\alpha = -1.3$ for C) between 10 MHz and 100 GHz and a value of 100 for the ratio of the total cosmic ray energy to the relativistic electron energy.

The results for components A and C are 6×10^{-4} G and 5×10^{-4} G, respectively. The relativistic pressures derived for A and C are 3×10^{-8} , and 2×10^{-8} dyn cm $^{-2}$, respectively. The thermal gas pressure of the emission-line region of NGC 7319, for which the electron density is $n_e=300-600$ cm $^{-3}$ (Aoki et al. 1996), is $4 - 8 \times 10^{-10}$ dyn cm $^{-2}$, assuming an electron temperature of $T_e = 10,000$ K. The relativistic pressure is thus at least one or two orders of magnitude higher than the thermal gas pressure.

4.2. Comparison of Radio Data with *HST* and Ground-based Spectroscopic Data

The absolute astrometric uncertainties for *HST* data are of the order of $1''$, so the *HST* image cannot be registered with the VLA images by relying on the internal *HST* astrometry. We

therefore attempted to obtain more accurate astrometric coordinates for the *HST* image using the following procedure. The *HST* image was rotated to the cardinal orientation by means of the keyword ‘ORIENTAT’ in the data header. Next, the image was smoothed with a gaussian function of $1''.5$ FWHM to simulate ground-based seeing. Various reasonable sizes of the gaussian were tried, but in all cases the positions of the peak agreed to $0''.1$. The peaks in the smoothed and unsmoothed images agree with each other to $0''.08$. We then assigned the absolute position of the nucleus determined by ground-based astrometry (Clements 1983) to the peak of the smoothed image.

However, this registration caused a systematic separation ($\sim 0''.7$) between features in the *HST* and radio images. The shift of $0''.7$ is larger than the internal errors of Clements’ (1983) and the VLA astrometry, but there can be uncertainties in Clements’ position due to structure in the nuclear region and the fact that the spectral sensitivity of Clements’ plates is different to the *HST* image. There are also systematic differences between the optical and radio astrometric frames. We finally decided to shift the optical peak onto the position of radio component B (Figs 1 and 2), while recognizing the somewhat arbitrary nature of this alignment and the consequent uncertainty in the interpretation which follows. The resulting shift of the original *HST* coordinates is $1''.26$. Using this registration, contours of the 3.6 cm radio image are overlaid on the *HST* image in Figure 6. Radio component A coincides with the northern arm of the spiral-like structure and component C is just inside of the V-shaped feature. Even with the alignment based on Clements’ nuclear position, radio component C is still to the NE of the V-shaped feature, so we regard this displacement as secure.

HST observations have revealed various associations between radio continuum and optical line-emission in Seyfert galaxies. In some Seyfert galaxies, the emission-line features are shell-like or arc-like and surround the radio emission; Mrk 573 is an excellent example (Capetti et al. 1996; Falcke, Wilson & Simpson 1998). This type of structure is interpreted as evidence that the ionized gas is compressed by the shocks created by the outward motion of the radio plasma. Such compression increases the gas density and enhances the surface brightness in line emission. The relationship between the V-shaped feature and radio component C is similar to that between the emission-line arcs and the radio hotspots in Mrk 573.

The emission-lines show a pronounced blueshift and the line profiles are flat-topped or double-peaked near the V-shaped feature (Fig. 7). There is also a blueward sloping asymmetry to the [O III] line profiles at the nucleus and northeast of the nucleus (Fig. 7).

We interpret these observational results as follows. The V-shaped feature represents compressed gas behind a bow shock driven into the photoionized gas by the outwardly moving radio component C. This compressed gas is given a motion outward by component C, and thus shows a large blueshift although there is not any independent evidence that the SW is the near side of the outflow yet. It is interesting that to the NE of component C, $[\text{N II}] 6584 > \text{H}\alpha$, while to the SW of component C, $\text{H}\alpha > [\text{N II}] 6584$ (Fig. 7). There thus appears to be a change of excitation

possibly associated with the bow shock. $H\alpha/[O III]$, however, does not significantly change across the position of component C when we reanalyzed the spectra of Aoki et al. (1996). This may be due to that each emission line was observed on different nights under different seeing conditions. More accurate observations are necessary to study change of excitation across component C. The blue wing in $[O III]$ at the nucleus and on the northeastern side of the nucleus may be related to the spiral-like structure in the HST image and/or components A and B in the radio images. This spiral-like structure could be a curved jet similar to that seen in ESO 428-G14 (Falcke et al. 1996) and NGC 4258 (Cecil, Wilson, & Tully 1992).

5. CONCLUSIONS

We have observed the Seyfert galaxy NGC 7319 with the VLA and found a triple radio source straddling the nucleus. We have also found a spiral-like structure and a V-shaped feature in an *HST* archival WFPC2 image of this galaxy. These optical features are closely related to the radio emissions. Combining these results with ground-based optical spectroscopy, we interpret the V-shaped feature as gas compressed by a bow shock driven into the ambient medium by the outwardly moving radio plasmoid. To confirm this interpretation, high resolution emission-line imaging and spectroscopy are needed.

We thank the staff of the Array Operation Center in Socorro, especially G. Taylor, for their kind help during observations and data reduction. We also thank Masaru Watanabe and Hiroshi Ohtani for their valuable suggestions and encouragements. Part of the data analysis was done at the Astronomical Data Analysis Center, National Astronomical Observatory of Japan, which is an inter-university research institute operated by Ministry of Education, Science, Culture and Sports. The National Radio Astronomy Observatory is a facility of the National Science Foundation operated under cooperative agreement by Associated Universities, Inc. This research was supported in part by NASA through grant NAG 81027.

REFERENCES

- Aoki, K., Ohtani, H., Yoshida, M., & Kosugi, G. 1996, *AJ*, 111, 140
- Bower, G. A., Wilson, A. S., Mulchaey, J. S., Miley, G. K., Heckman, T. M., & Krolik, J. H. 1994, *AJ*, 107, 1686
- Bower, G. A., Wilson, A. S., Morse, J. A., Gelderman, R., Whittle, M., & Mulchaey, J. 1995, *ApJ*, 454, 106
- Capetti, A., Axon, D. J., Macchetto, F. D., Sparks, W. B., & Boksenberg, A. 1996, *ApJ*, 469, 554
- Capetti, A., Macchetto, F. D., & Lattanzi, M. G. 1997, *ApJ*, 476, L67

- Cecil, G., Wilson, A. S., & Tully, R. B. 1992, *ApJ*, 390, 365
- Clements, E. D. 1983, *MNRAS*, 204, 811
- Falcke, H., Wilson, A. S., Simpson, C., & Bower, G. A. 1996, *ApJ*, 470, L31
- Falcke, H., Wilson, A. S., & Simpson, C. 1998, *ApJ*, 502, 199
- Haniff, C. A., Wilson, A. S., & Ward, M. J. 1988, *ApJ*, 334, 104
- Kaftan-Kassim, M. A., Sulentic, J. W., & Sistol, G. 1975, *Nature*, 253, 176
- Kukula, M. J., Pedlar, A., Baum, S. A., & O’Dea, C. P. 1995, *MNRAS*, 276, 1262
- Smoot, G. F., Bennett, C. L., Kogut, A., Aymon, J., Backus, C., de Amici, G., Galuk, K., Jackson, P. D., Keegstra, P., Rokke, L., Tenorio, L., Torres, S., Gulkis, S., Hauser, M. G., Jansen, M. A., Mather, J. C., Weiss, R., Wilkinson, D. T., Wright, E. L., Boggess, N.W., Cheng, E. S., Kelsall, T., Lubin, P., Meyer, S., Moseley, S. H., Murdock, T. L., Shafer, R. A., Silverberg, R. F. 1991, *ApJ*, 371, L1
- Ulvestad, J. S., & Wilson, A. S. 1984, *ApJ*, 278, 544
- Ulvestad, J. S., & Wilson, A. S. 1984, *ApJ*, 285, 439
- Ulvestad, J. S., & Wilson, A. S. 1989, *ApJ*, 343, 659
- van der Hulst, J. M., & Rots, A. H. 1981, *AJ*, 86, 1775
- Whittle, M., Pedlar, A., Meurs, E. J. A., Unger, S. W., Axon, D. J., & Ward, M. J. 1988, *ApJ*, 326, 125

Fig. 1.— The 3.6 cm naturally weighted image of NGC 7319. The compact components are labeled A, B, and C. The beam size is $0''.27 \times 0''.26$ FWHM.

Fig. 2.— Same as Figure 1, but for the 6 cm naturally weighted image. The beam size is $0''.47 \times 0''.45$ FWHM.

Fig. 3.— Same as Figure 1, but for the 20 cm uniformly weighted image. The beam size is $1''.31 \times 1''.29$ FWHM. Components A and B are merged together by the lower resolution than attained at 3.6 and 6 cm.

Fig. 4.— *HST* WFPC2 F606W image of NGC 7319. North is up, and east is to the left. The field of view is $10'' \times 10''$.

Fig. 5.— Fine scale structure in the *HST* WFPC2 F606W image of NGC 7319. The image was made by subtracting a smoothed image from the original *HST* image (see text). North is up, and east is to the left. The field of view is $10'' \times 10''$, so the spatial scale is the same as Figure 4.

Fig. 6.— Contours of the VLA 3.6 cm map are overlaid on the *HST* F606W image. The two images were registered by assuming that radio component B corresponds to the peak in the *HST* F606W image (see text).

Fig. 7.— The variations of line profile along P.A. 27° . (*Left*) The ‘ladder’ overlaid on the 3.6 cm VLA image of NGC 7319 shows the slit. Each small rectangle corresponds to a $1''.8 \times 1''.46$ slit increment. (*Center*) [O III] $\lambda 5007$ profiles from Aoki et al. (1996). The northeast and southwest ends of the slit are indicated. The numbers on the left give slit increment numbers. The arrows on the right mark positions of the radio components A, B, the optical continuum peak, the radio component C and the V-shaped feature, respectively. The spatial and velocity scales are indicated. The small tick marks indicate 1000 km s^{-1} intervals. The long tick mark indicates the systemic velocity of 6740 km s^{-1} . (*Right*) Same as (*Center*), but $\text{H}\alpha + [\text{N II}] \lambda\lambda 6548, 6583$ profiles.

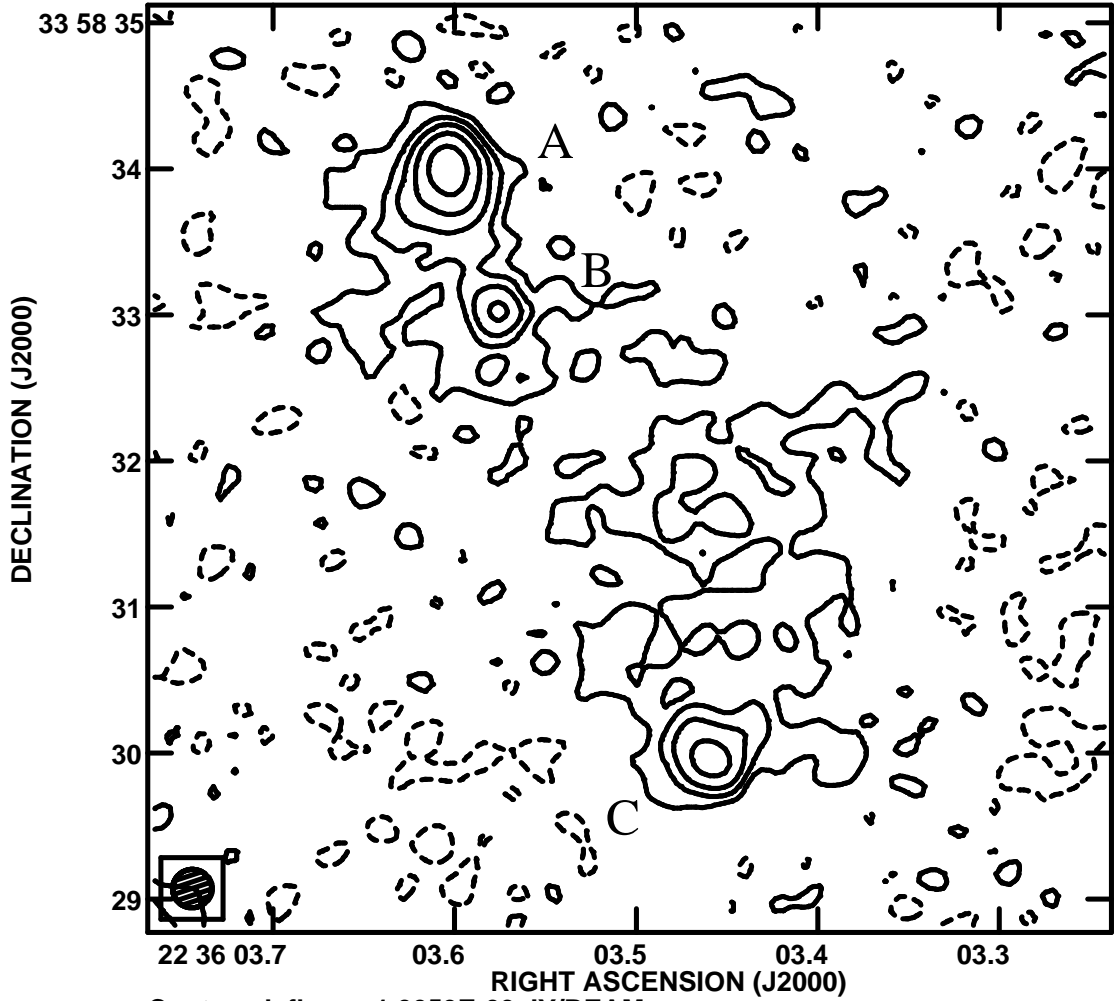
Table 1. Parameters of the radio components in NGC 7319

	α^a J2000 (22h36m+)	δ^a J2000 (33°58'+)	3.6 cm f_ν (mJy)	3.6 cm Size (")	6 cm f_ν (mJy)	6 cm Size (")	20 cm f_ν (mJy)	Spectral index 3.6-6 cm	Spectral index 6-20 cm
A	03.604s	33'95	2.1	0.3×0.2	4.1	0.4×0.3	19 ^b	-1.2	–
B	03.578s	33'04	0.5	–	1	–	–	-1.4	–
C	03.460s	30'02	0.9	0.25×0.2	1.8	0.5×0.4	9	-1.3	-1.3

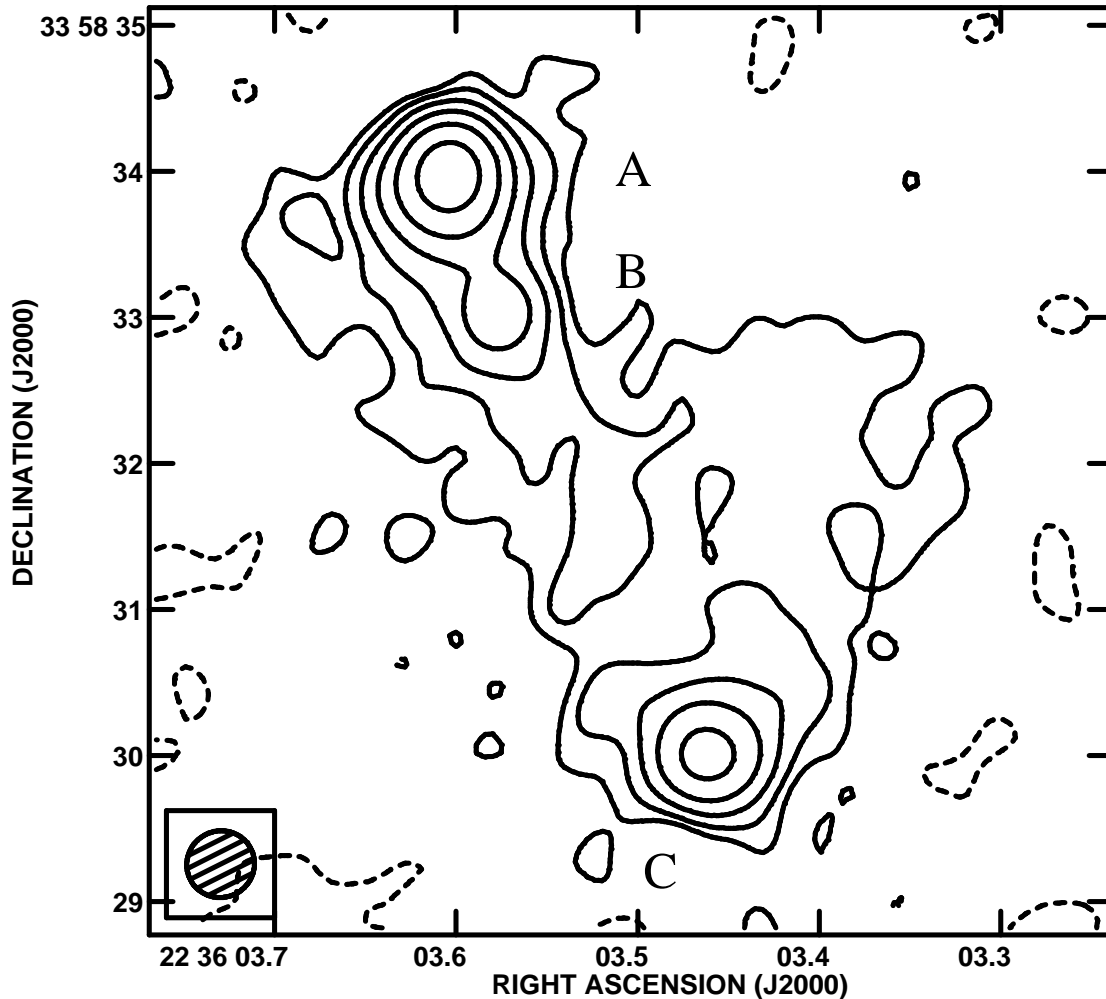
^aThese are mean of 3.6 and 6 cm values.

^bThis is the sum of the components A and B.

CONT: NGC7319 IPOL 8439.900 MHZ NGC7319-XNA.ICLN.1

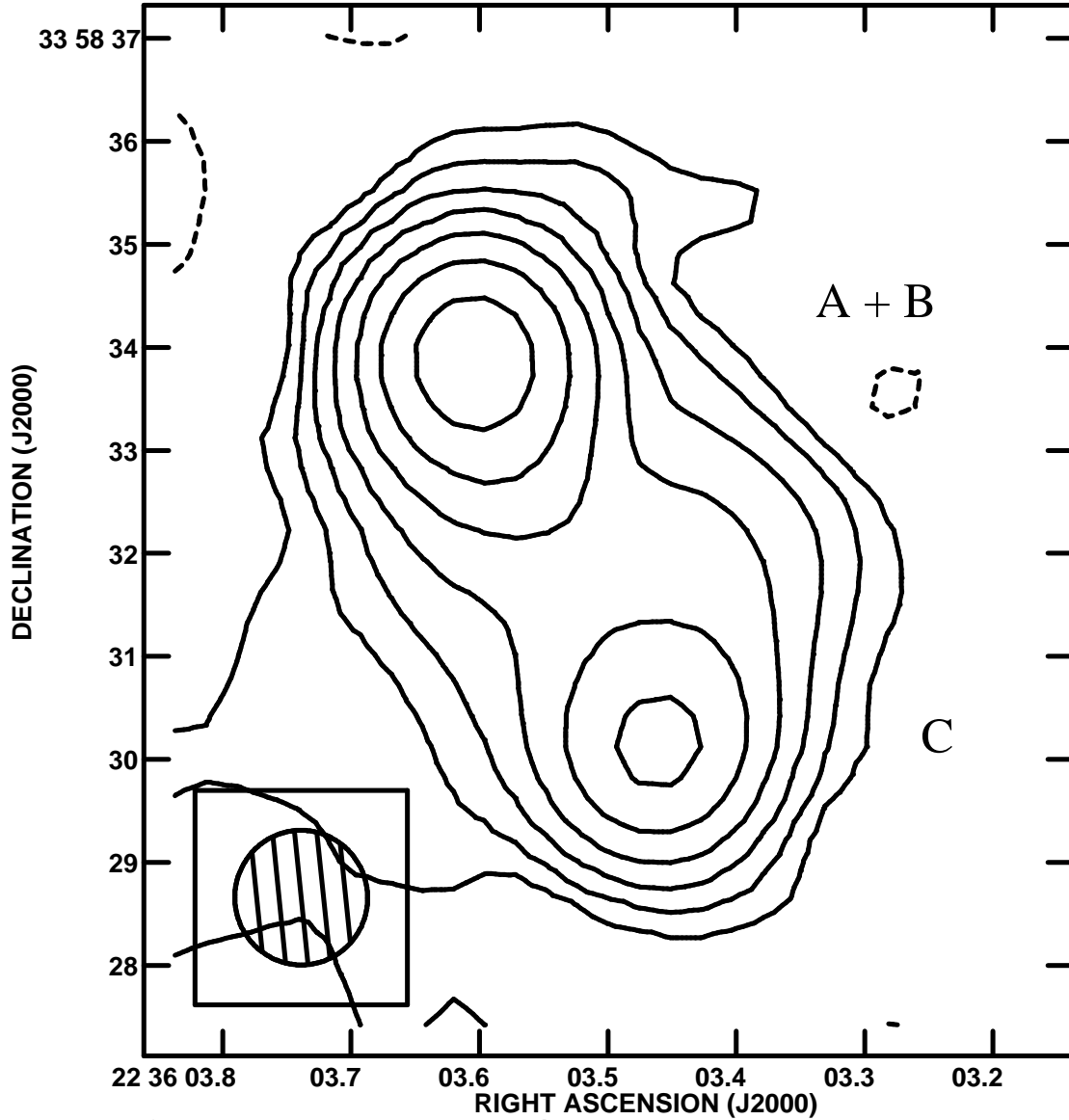


CONT: NGC7319 IPOL 4860.100 MHZ NGC7319-CNA.ICLN.1

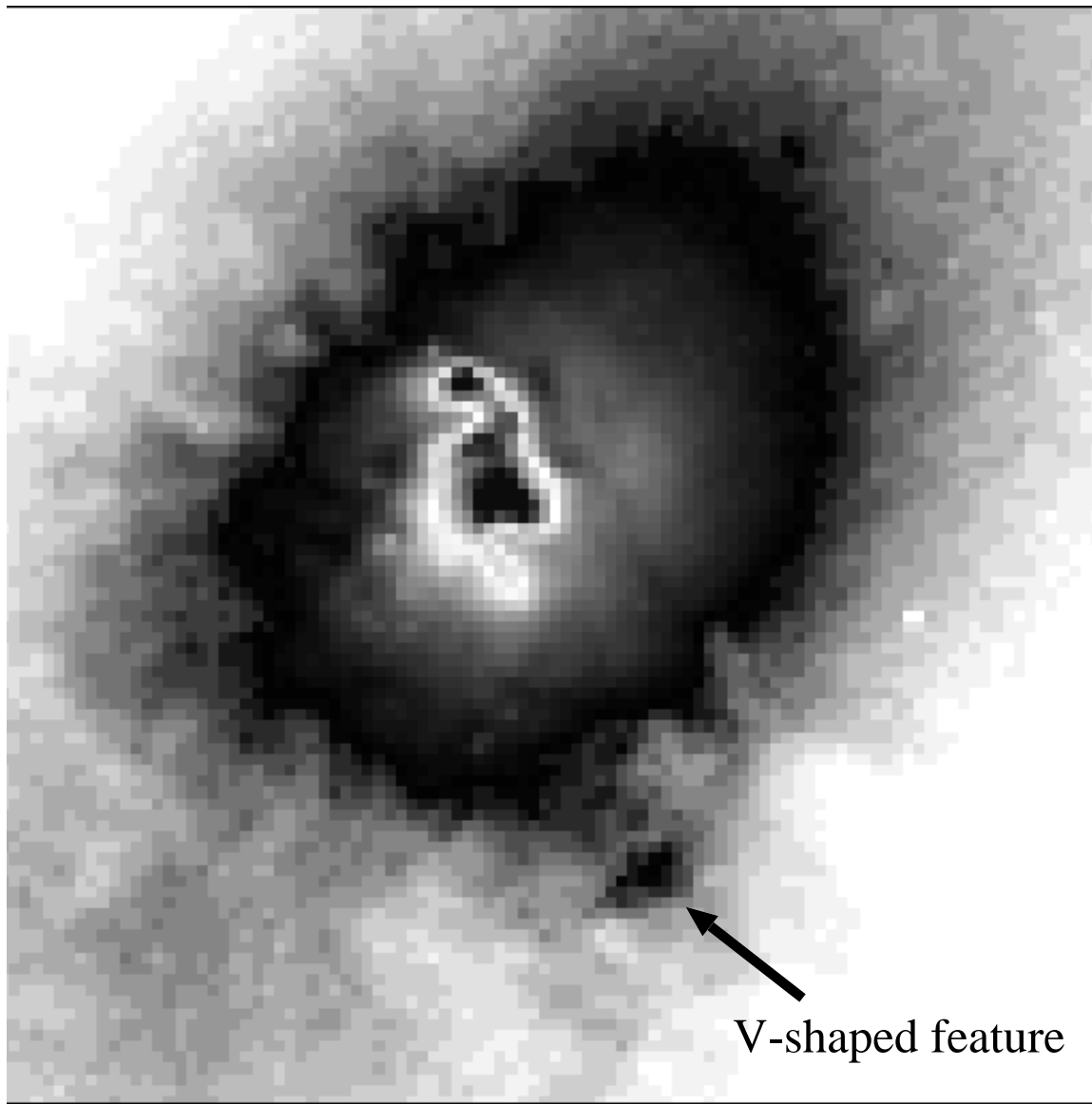


Cont peak flux = 2.6017E-03 JY/BEAM
Levs = 5.2034E-05 * (-0.500, 1.000, 2.000,
4.000, 8.000, 16.00, 32.00)

CONT: NGC7319 IPOL 1400.000 MHZ NGC7319LUN.ICLN.1



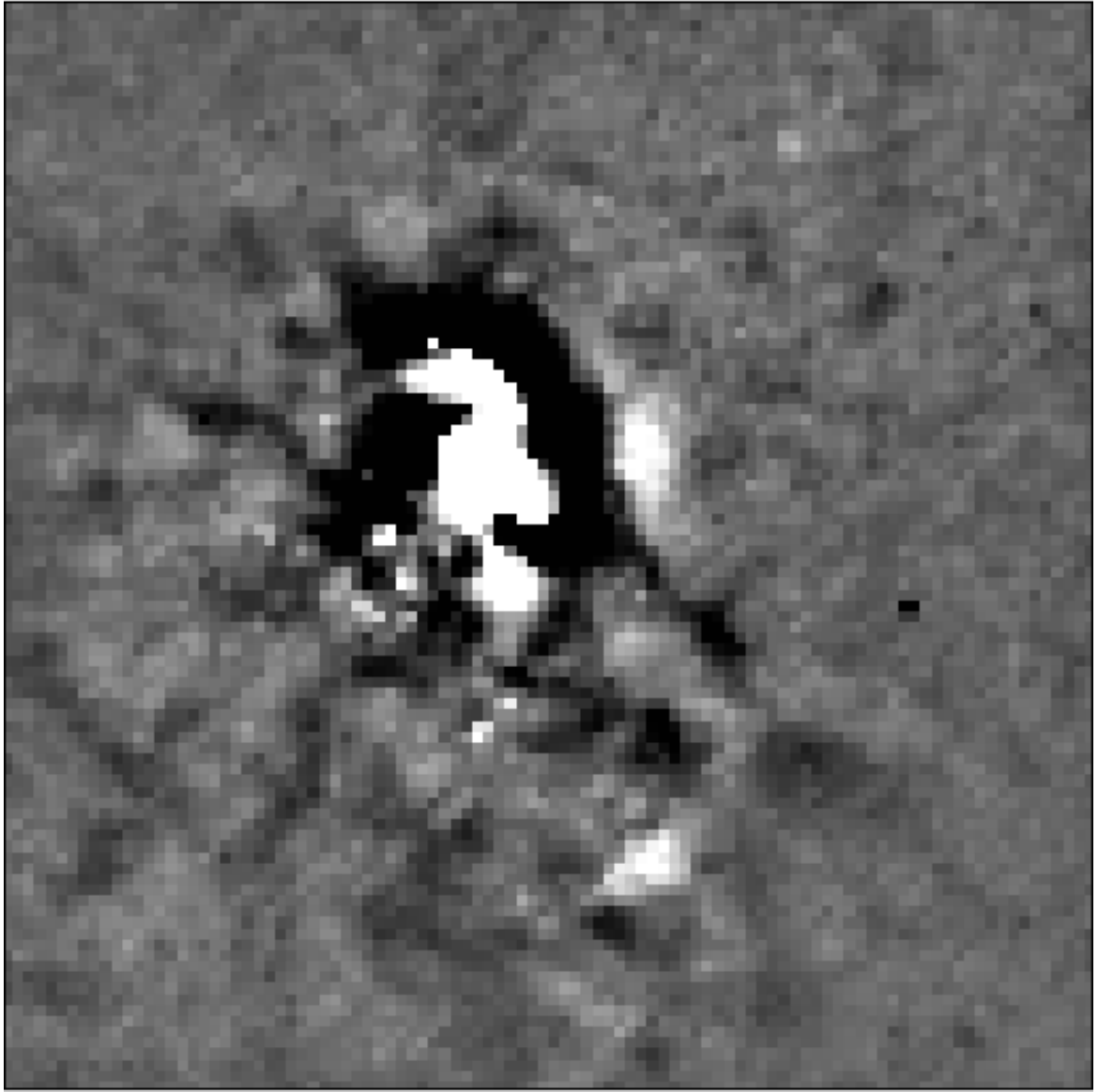
Cont peak flux = 1.2111E-02 JY/BEAM
Levs = 1.2111E-04 * (-0.500, 1.000, 2.000,
4.000, 8.000, 16.00, 32.00, 64.00)



20

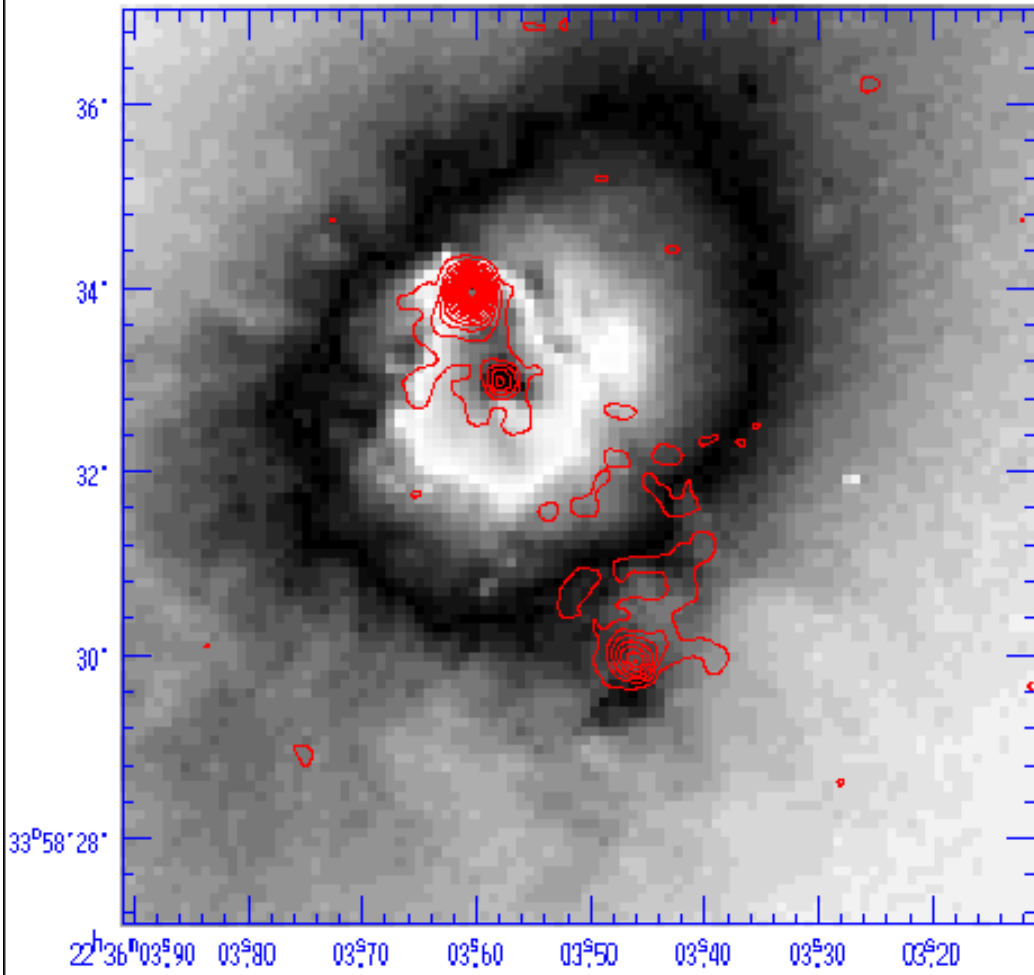
relative intensity

1000



-30 relative intensity 30

NGC 7319



relative intensity

20

1000

[O III] 5007

H α [N II]

